Evolution of Microstructure during Shear Alignment in a Polystyrene–Polyisoprene Lamellar Diblock Copolymer

V. K. Gupta, R. Krishnamoorti, and J. A. Kornfield*

Chemical Engineering 210-41, California Institute of Technology, Pasadena, California 91125

S. D. Smith

Procter & Gamble, Cincinnati, Ohio 45239

Received January 20, 1995; Revised Manuscript Received March 21, 1995[⊗]

ABSTRACT: The process of flow-induced alignment in a lamellar diblock copolymer melt is investigated using simultaneous measurements of shear stress and birefringence. Flow birefringence, *in situ*, during oscillatory shear clarifies how the orientation distribution evolves toward either "parallel" or "perpendicular" alignment, i.e., layers normal to either the velocity gradient or the vorticity axis, respectively. A nearly symmetric, polystyrene–polyisoprene diblock (ODT ≃ 164 °C) is studied at 120 °C ($T/T_{ODT} \simeq 0.90$). The critical frequency (ω_c') associated with a crossover in the relaxation dynamics from being dominated by the macromolecular response to being dominated by the microstructural response is estimated to be $\omega_c' \approx 3-7$ rad/s at 120 °C. At high frequencies (relative to ω_c'), shearing induces parallel alignment, while shearing at lower frequencies leads to perpendicular alignment. In all cases, alignment proceeds through a "fast" process followed by a "slow" one. The fast process is dominated by depletion of the projection of the orientation distribution along either the perpendicular direction or the "transverse" direction (layers normal to the flow). The resulting biaxial distribution is transformed into a well-aligned uniaxial one during the slow process. Surprisingly, the projection along the perpendicular direction can disappear *faster* than the projection along the transverse direction. This occurs during the fast process en route to parallel alignment with sufficiently high frequencies. As the shearing frequency is lowered, the projection along transverse orientation decreases faster than that along the perpendicular direction.

1. Introduction

Block copolymers provide excellent model systems to understand the complex morphological and dynamical response of microstructured materials, including liquid crystals, surfactants, and colloids.[1] Microphase-separated block copolymers, in a variety of microstructures, have been shown to adopt "single-crystal"-like order when subjected to symmetry-breaking fields, such as electric fields and flow fields.[2-9] In particular, for lamellar diblock copolymers it has been shown that two states of macroscopic order can be achieved by large-amplitude oscillatory shear. Shearing at different frequencies but at the same temperature and strain amplitudes[5,6] can produce alignment either with layer normals along the shear gradient direction (parallel) or with layer normals along the vorticity direction (perpendicular) (Figure 1). In spite of considerable theoretical and experimental work, the mechanisms as well as the controlling parameters for flow-induced alignment in block copolymers remain unresolved.

Much of the experimental work has focused on two classes of systems: (a) polystyrene–polydiene block copolymers (where the diene may be either butadiene or isoprene) with the components having vastly different glass transition temperatures and experimental temperatures not much greater than the glass transition temperature of the styrene-rich phase[2-4,10-14] and (b) well-entangled, polyolefin diblocks, such as PE–PEE, PE–PEP, and PEE–PEP (PE = polyethylene, PEE = poly(ethylethylene), and PEP = poly(ethylene-*alt*-propylene)) wherein the components have similar glass transition temperatures and flow alignment is performed at temperatures much greater than either component glass transition temperature.[5,6,15-17]

The early shear experiments on lamellar styrene–diene block copolymers induced alignment in the parallel direction,[3,4] but more recent experiments on polyolefin diblocks showed that perpendicular alignment could also be produced.[5] Koppi and coworkers[5] found

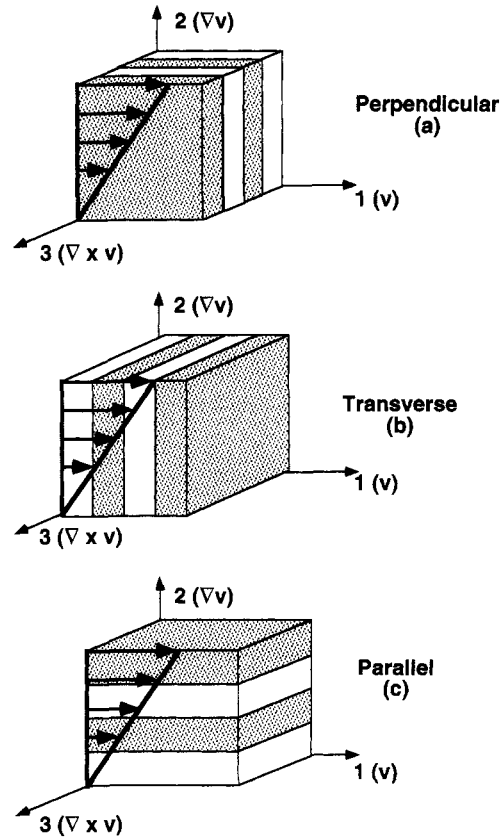

Figure 1. Schematics of macroscopically ordered lamellar diblocks: (a) perpendicular; (b) transverse; (c) parallel.

[⊗] Abstract published in *Advance ACS Abstracts,* May 1, 1995.

0024-9297/95/2228-4464$09.00/0

that for lamellar polyolefin diblocks, large-amplitude reciprocating deformations at shear frequencies in the dynamic regime dominated by the layered microstructure and at temperatures near the order–disorder transition resulted in perpendicular alignment, while parallel alignment was produced at lower reduced shear frequencies over a broader range of temperatures. More recently, Winey and co-workers,[10–12] working with a polystyrene–polyisoprene (PS–PI) lamellar diblock (12.5K–9.5K, T_{ODT} = 152 °C), achieved perpendicular alignment near the order–disorder transition (*e.g.*, ω = 10 rad/s, T = 144 °C, γ_0 = 100%) and parallel alignment at lower temperatures (*e.g.*, ω = 0.1–100 rad/s, T = 98 °C, γ_0 = 2–5%). This differed from the polyolefin case wherein parallel alignment was restricted to lower reduced frequencies than those inducing perpendicular alignment.

In early studies,[3,4] where only parallel alignment was found, it was proposed that flow alignment could proceed by mechanisms that include grain rotation, selective melting of grains, and defect migration. To explain the occurrence of parallel as well as perpendicular alignment, Koppi and coworkers[5] speculated that perpendicular alignment was achieved because "the interfacial material is deformed by the vorticity component of the velocity gradient in all but the perpendicular orientation". In contrast, they argued that parallel alignment occurred by "breaking and reforming the lamellae individually through the movement of dislocations (or disclinations)".

These ideas about alignment mechanisms were based primarily on the microstructure observed after alignment using small-angle neutron scattering (SANS),[5] transmission electron microscopy (TEM), and small-angle X-ray scattering (SAXS).[10,11] Apart from the possibility of artifacts induced during the cooling, cutting, and mounting processes for sample preparation, such characterization does not provide any information on the molecular and microstructural dynamic responses during flow alignment. This information is vital to formulate mechanisms of flow alignment and to discriminate among existing ideas. Thus, real time, *in-situ* studies are essential to understanding the mechanism of flow alignment—a prerequisite for rational control of the macroscopic ordering in block copolymers and other mesostructured materials.

Studies with a focus on *in-situ* measurements during shearing of block copolymers have recently appeared in the literature.[17–19] However, the SANS and SAXS studies[18,19] by Balsara *et al.* and Okamoto *et al.* report scattering profiles averaged over periods of several minutes (~8–20 min) and track changes in the microstructure on a coarse time scale. Both investigations only examine a few conditions of alignment. In contrast, the *in-situ* stress-optical study by Kannan *et al.* examines alignment processes with a much higher time resolution (~0.1 s).[17] However, in their polymer, a PEP–PEE diblock, flow birefringence is sensitive to chain orientation, since the intrinsic contribution dominates; at high frequencies, where conformation distortion occurs, this precludes determination of the lamellar orientation distribution during development of perpendicular alignment.

To investigate the dynamics of the processes that lead to both parallel and perpendicular alignment, we apply *in-situ* rheooptical methods to a system in which the form contribution dominates the birefringence, a lamellar PS–PI melt. This permits study of the coherent macroscopic order as it develops during oscillatory shear. The higher time resolution of rheooptical measurements proves extremely valuable as significant changes in microstructure occur initially within times of less than a minute. Using transient birefringence measurements, we perform a systematic study of the effects of shear frequency, strain amplitude, and temperature on the rate, the route, and the final direction of alignment. In this paper, we focus on the effect of shear frequency.

In the following section, we describe the material and the rheooptical methods used to simultaneously characterize transient microstructural alignment and macroscopic viscoelastic properties. In section 3 we present observations during shear orientation. Section 4 includes interpretation of the transient birefringence and dynamic modulus in terms of a proposed trajectory of microstructure evolution during shear alignment and a brief discussion of the results in the context of the mechanisms that have been suggested in the literature.

2. Experimental Section

A. Materials, Apparatus, and Methods. A nearly symmetric polystyrene–polyisoprene diblock copolymer with $M_w \simeq 20\,000$, and $M_w/M_n \leq 1.06$ was prepared by anionic synthesis using standard techniques. Clean material was obtained by filtering a solution of the polymer in toluene through a 0.2 μm Teflon filter, followed by precipitation in methanol and vacuum drying. Rheological determination[20] of the order–disorder transition temperature indicated $T_{ODT} \simeq 164$ °C.

The mechanical and optical properties of this block copolymer were characterized using a rheooptical apparatus uniquely suited for simultaneous, quantitative measurements of dynamic stress and birefringence over a wide range of frequencies (0.01–100 rad/s) and temperatures (−100 to +400 °C). The construction of this apparatus, the instrumentation, and data acquisition are described in detail elsewhere.[22,23] All experiments were performed under an inert nitrogen atmosphere using the "shear-sandwich" geometry, with light propagation along the velocity gradient direction (axis 2). This allowed us to measure the projection of the anisotropic refractive index tensor in the plane formed by the flow direction (axis 1) and the vorticity axis (axis 3). The present rheooptic instrument measures the sign of birefringence along with its magnitude. Experiments were performed with the sample loaded in a tool with a gap of 0.26 mm and rectangular plates (15.92 × 12.65 mm). The optical path length was twice the gap width, *i.e.*, 0.52 mm. A red helium–neon laser at a wavelength of 633 nm was used.

For a highly birefringent sample (with little or no dichroism), the measurable optical property was sin μ, where the retardation $\mu = (2\pi d/\lambda)\,\Delta n_{ij}$, with d the optical path length, λ the wavelength of the incident light, and Δn_{ij} the birefringence in the i,j-plane (1,3-plane in our work). Because the principal value of μ was obtained by inverting the sine function, errors are large in the vicinity of $\mu = (2m + 1)\pi/2$. However, the uncertainty in the precise value of μ in the time intervals where μ is near $(2m + 1)\pi/2$ does not alter the conclusions of this work.

We used two types of oscillatory shear protocols: (1) frequency sweeps at strain amplitudes small enough to characterize the linear viscoelastic response of the sample before and after alignment and (2) prolonged, large-amplitude (10% ≤ γ_0 ≤ 110%) oscillatory shear at a fixed frequency and temperature to induce macroscopic alignment of the microstructure. In this paper we describe alignment experiments carried out at a single temperature of 120 °C. This choice of temperature permitted us to explore shear alignment to both parallel *and* perpendicular alignment with various shear frequencies and a wide range of strain amplitudes. To establish a reproducible initial condition before each alignment experiment, the sample was heated well into the disordered

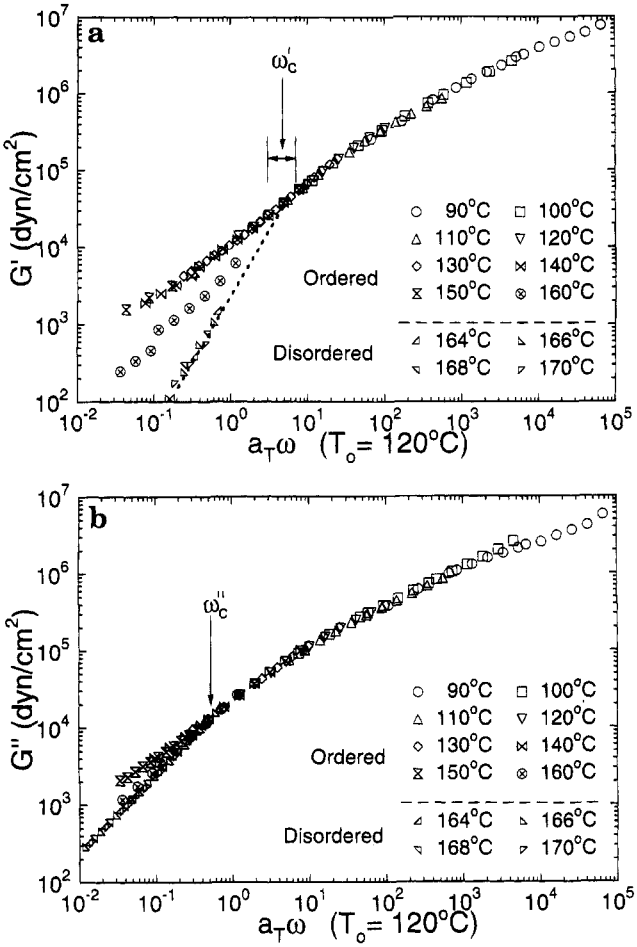

Figure 2. (a) Storage, G', and (b) loss, G'', moduli on a shifted frequency scale (T_0 = 120 °C, a_T given in Table 1) for an ordered (T < 164 °C) but macroscopically unaligned state and the disordered (T > 164 °C) melt. The lateral bar in a indicates the approximate value of the critical frequency ω_c' (see text).

phase (180 °C) and allowed to equilibrate at the temperature for 15–20 min. The sample was then cooled to the desired temperature in the ordered state and equilibrated for 15 min. This procedure resulted in a reproducible initial state, confirmed by frequency sweep measurements before each alignment process.[24] Once the sample was loaded in the shearing tool, uninterrupted measurements over several weeks were carried out by simply cooling and reheating the same sample to minimize relative errors (*e.g.*, variations in sample thickness in successive experiments, optical-train calibration, etc.). Clean terminal behavior in the disordered state after completion of the whole suite of experiments (Figure 2) and GPC traces of the sample showed no evidence of any thermal or oxidative degradation, or cross-linking. Furthermore, we saw neither a broadening nor a shifting of the T_{ODT} over the course of weeks of experimentation.

B. Stress and Birefringence. In shear flow, by symmetry, the shear stress (σ_{12} in the coordinate system described above) is an odd function of the strain. For oscillatory shear $\gamma(t) = \gamma_0 \sin \omega t$, if γ_0 is small, the leading term in an expansion of $\sigma_{12}(t)$ in the harmonics of ω dominates. Thus, σ_{12} is expected to be sinusoidal with the same frequency (ω) as the applied strain. When this is the case and when the stress is linear in the strain, we can define storage and loss moduli $G'(\omega)$ and $G''(\omega)$: $\sigma_{12} = \gamma_0[G' \sin \omega t + G'' \cos \omega t]$.

Frequency sweeps to characterize the linear viscoelastic behavior of the block copolymer were performed with small enough strain amplitudes to avoid macroscopic alignment and nonlinearity in the stress response. However, this was particularly difficult to achieve at elevated temperatures where larger strains were required to obtain a measurable force response.

Table 1. Frequency Shift Factors for PS–PI in the Ordered but Macroscopically Unaligned State

T (°C)	a_T (T_0 = 120 °C)	T (°C)	a_T (T_0 = 120 °C)
90	660	160	0.0114
100	45.5	164	0.0068
110	5.5	166	0.006
130	0.24	168	0.005
140	0.077	170	0.0045
150	0.034		

In contrast, during "flow alignment" we used strain amplitudes large enough to produce alignment of the lamellae but small enough that the stress was dominated by the fundamental Fourier component and could be described using an effective dynamic modulus G^*_{eff} that changed with time during prolonged shearing. The higher harmonics (3ω, 5ω) in the stress response were also recorded.[25]

For PS–PI diblocks in the strongly segregated regime, the form contribution to the birefringence ($\Delta\mathbf{n}_f$) resulting from the block copolymer microstructure is estimated to be at least 3 times the intrinsic or "molecular" contribution ($\Delta\mathbf{n}_i$).[26,27] Therefore, in our experiments we expect the form birefringence to dominate: consequently, the observed birefringence provides a measure of the lamellar orientation distribution. A beam propagating along the velocity gradient probes the projection of $\Delta\mathbf{n}$ on the 1,3-plane, $\Delta\mathbf{n}_{13}$. Due to flow symmetry, the principal axes of $\Delta\mathbf{n}_{13}$ coincide with axes 1 and 3, so its anisotropy is completely described by the magnitude of the birefringence $\Delta n_{13} = n_{11} - n_{33}$. If a particular orientation of the projection of the lamellar normal in the 1,3-plane were enhanced by oscillatory shear, it would be directed along one of the axes (1 or 3) and would be manifested in Δn_{13}. Thus, the evolution of the steady offset in $\Delta n_{13}^{(d)}$ is sensitive to the development of alignment. In the parallel orientation, the lamellar normal ($\hat{u}$) points in the velocity gradient direction (axis 2) and is along the beam propagation direction. This results in a zero birefringence in the 1,3-plane for a perfectly aligned parallel state.[30] In contrast, in perpendicular alignment the layer normal ($\hat{u}$) points along the vorticity direction (axis 3); for PS–PI, this corresponds to positive Δn_{13}, since the form contribution has a higher index along the layers. Similarly, a large, negative 1,3-birefringence corresponds to the "transverse" orientation, with layer normal ($\hat{u}$) along the flow direction (axis 1).

3. Results

A. Dynamic Moduli of Disordered and Unaligned Ordered Phases. Time–temperature superposition at a reference temperature of 120 °C was used to construct dynamic moduli, G' and G'', master curves that span nearly 7 decades in reduced frequency (Figure 2). The data measured at different temperatures using small-amplitude oscillatory shear[32] were shifted only along the frequency scale to construct the master curves (a_T reported in Table 1). The dynamic moduli at temperatures near and above the ODT are also shown in the same figure.[33]

In the ordered phase, both G' and G'' roughly follow a power law scaling with frequency,[12,16,34,35] which can be approximated as $\omega^{0.5-0.7}$. The disordered state dynamic moduli show typical homopolymer-like terminal behavior with $G' \propto \omega^2$ and $G'' \propto \omega^1$ (Figure 2).

We define two critical frequencies below which the relaxation dynamics are hypothesized to be dominated by relaxation modes of the microdomain structure.[16] The critical frequency based on the loss modulus (ω_c'') is taken to be the frequency below which the ordered and disordered loss moduli fall on different curves: $\omega_c'' \approx$ 0.5 rad/s at T = 120 °C. For the storage modulus, we estimate the value of ω_c' by extrapolating the disordered state data ($\omega_c' \approx$ 3–7 rad/s at T = 120 °C;

Figure 2a). The uncertainty results from the rather long extrapolation of the disordered state data required to estimate ω_c'.

B. Evolution of Birefringence and Dynamic Modulus during Alignment. Flow alignment experiments reported here were carried out over a range of shear frequencies at a single temperature of 120 °C. The final state of alignment was characterized by the birefringence (Δn_{13}) and the small strain moduli. In agreement with earlier work[10-13] we found two distinct regions of parallel and perpendicular alignment.[36] At high shear frequencies relative to the critical frequency ω_c' (*i.e.*, $\omega \geq 10$ rad/s at 120 °C) parallel alignment was achieved, and at lower frequencies perpendicular alignment was induced (*i.e.*, $\omega \leq 1$ rad/s at 120 °C).

1. Perpendicular Alignment. Shearing at $\omega = 1$ rad/s, $\gamma_0 = 1$ produced a rapid rise in $\Delta n_{13}^{(d)}$ followed by a slow saturation to $\sim 8 \times 10^{-4}$ (Figure 3a). Further confirmation of the final magnitude of the birefringence was obtained from the color observed on viewing the sample through crossed polarizers under white light and using the Michél Levy color scheme.[37] While it is difficult to evaluate the order parameter from the birefringence, there are indications that it is quite high. Recent calculations[26,27] for lamellar styrene–diene block copolymers in the strong segregation limit suggest a value of $\Delta n \approx 16 \times 10^{-4}$ for a perfectly aligned sample. However, the condition examined here is in the weak segregation limit, resulting in smaller (form and intrinsic) birefringence than a strongly segregated PS–PI. It should be noted that, in a large suite of experiments using different strain amplitudes[38] and reduced frequencies, we have never observed the final birefringence of the perpendicular state to exceed $\Delta n_{13,max} \simeq 10 \times 10^{-4}$.

The effective dynamic moduli during shear alignment showed an initial rapid fall, followed by a gradual decrease to a steady value (Figure 3b). Small strain frequency sweeps before and after shear showed that alignment resulted in a much stronger frequency dependence for both G' and G'' (Figure 3c) and significantly lower dynamic moduli at low frequencies.

To examine the relationship between microstructure and macroscopic mechanical properties, in a separate experiment large-amplitude shearing was interrupted to measure the dynamic moduli (linear viscoelastic response) at different points during the course of alignment. The storage and loss moduli drop monotonically as alignment proceeds to point c on Figure 3a, with the largest drop occurring between points b and c. Beyond point c the trend changes, with G' remaining essentially unchanged and G'' increasing from point c to d to e. These results are summarized in the Appendix (Figure 7).

2. Parallel Alignment. Shearing at 100 rad/s ($\gamma_0 = 0.5$) and at 10 rad/s ($\gamma_0 = 0.8$) produces parallel alignment of the lamellae. Surprisingly, while the final states in both the shear alignment experiments exhibit $\Delta n_{13}^{(d)} \simeq 0$, the evolution of birefringence during alignment is dramatically different (Figure 4a). At $\omega = 100$ rad/s, $\Delta n_{13}^{(d)}$ rapidly becomes large and *negative*, in stark contrast to the steep *positive* rise in $\Delta n_{13}^{(d)}$ for $\omega = 10$ rad/s. A positive $\Delta n_{13}^{(d)}$ implies enhanced lamellar orientations biased toward perpendicular alignment relative to those biased along the transverse direction. Conversely, a negative $\Delta n_{13}^{(d)}$ implies a diminished ratio of the projection of perpendicular orientation to transverse orientation—quite contrary to expectations.

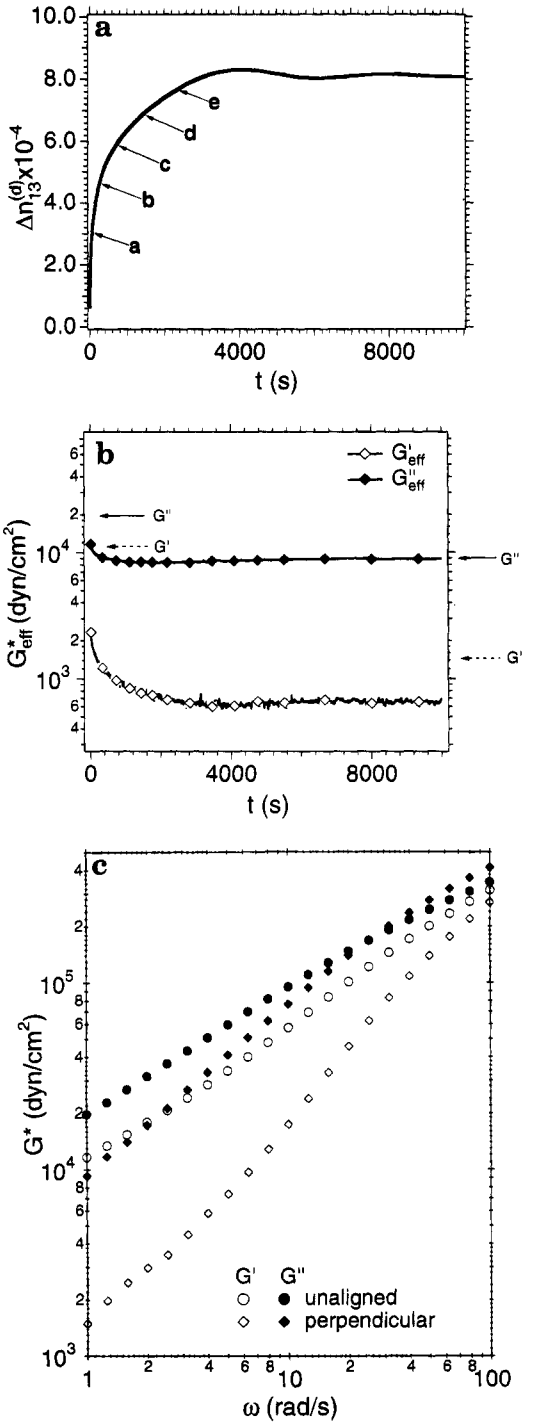

Figure 3. (a) Evolution of the steady offset in 1,3-birefringence during large-amplitude shear alignment at $T_0 = 120$ °C and $\omega = 1$ rad/s ($\gamma_0 = 1.0$) to a perpendicular aligned state. The letters mark approximate locations where, in a separate set of experiments, shear alignment was stopped to perform small strain measurements of the dynamic moduli (see Figure 7a,b). (b) Evolution of effective storage and loss moduli during the large-amplitude shear alignment experiments described in part a. Sparsely spaced markers have been used to distinguish the curves. The arrows at the left and right indicate the small strain dynamic moduli at $\omega = 1$ rad/s, before and after shearing, respectively. (c) Dynamic moduli at $T_0 = 120$ °C obtained using small strain oscillatory shear measurement before and after large-amplitude shear as in part a.

For both sets of flow conditions, the maximum absolute value of birefringence $|\Delta n_{13}^{(d)}| \approx {}^1/_3 \Delta n_{13,max}$ ($\sim 3 \times 10^{-4}$) and is reached within ~ 100 s. Both these initial

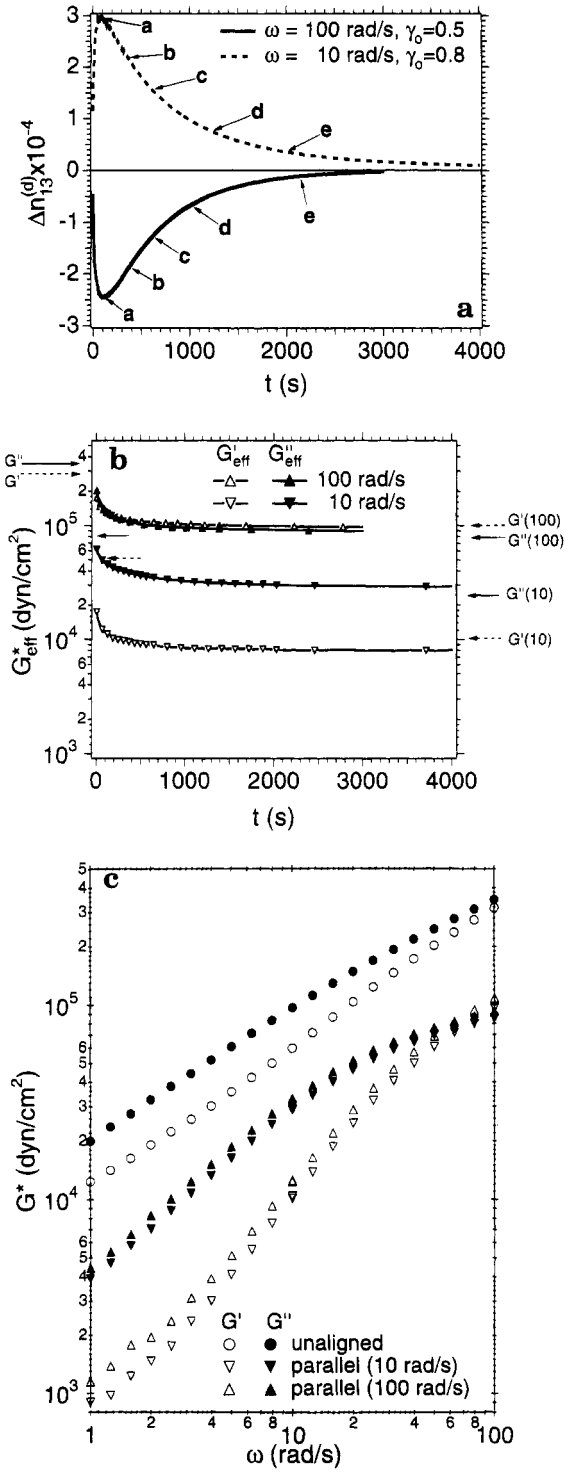

Figure 4. (a) Evolution of the steady offset in 1,3-birefringence during large-amplitude shear alignment at $T_0 = 120$ °C, $\omega = 10$ rad/s ($\gamma_0 = 0.8$), and 100 rad/s ($\gamma_0 = 5$) to a parallel aligned state. The letters mark approximate locations where, in a separate set of experiments, shear alignment was stopped to perform small strain measurements of the dynamic moduli (see Figure 8a–d). (b) Evolution of effective storage and loss moduli during the large-amplitude shear alignment experiments described in part a. Sparsely spaced markers have been used to distinguish between the curves. The arrows at the left and right indicate the small strain dynamic moduli at 10 or 100 rad/s, as indicated, before and after shearing, respectively. (c) Dynamic moduli at $T_0 = 120$ °C obtained using small strain oscillatory shear measurement before and after large-amplitude shear as in part a.

fast processes are followed by a much slower ($t \sim 3000$–4000 s) decrease of birefringence to a near zero value. This peak value of $\Delta n_{13}^{(d)} \sim 3 \times 10^{-4}$ for the case of red HeNe radiation ($\lambda = 633$ nm) and the geometry employed ($d = 0.52$ mm) corresponds to a retardation $\mu \approx \pi/2$. Since we measure $\sin \mu$, an increase in μ beyond $\pi/2$ to a value of π is indistinguishable from a decrease of μ from $\pi/2$ to 0. Therefore, shearing experiments were repeated using green HeNe radiation ($\lambda = 543$ nm) to verify the magnitude of the birefringence. These experiments confirm that the birefringence indeed reaches a maximum magnitude of $\approx 3 \times 10^{-4}$ and then decreases to nearly zero.

The effective dynamic moduli during shear show a large initial drop followed by a gradual flattening out (Figure 4b). This drop is slightly larger than that during perpendicular alignment at 1 rad/s. The small strain dynamic moduli for the two aligned samples are also nearly identical to each other and dramatically lower than those of the unaligned ordered sample (Figure 4c) as well as the perpendicular aligned sample (*cf.* Figure 3c). A similar decrease in dynamic moduli has been reported for parallel alignment in PS–PI.[10–12] These dynamic moduli measurements, together with the small value of 1,3-birefringence at the end of shearing, allow us to infer that the final alignment is along the parallel direction.

As before, to study the link between the microstructure and the macroscopic mechanical behavior, we performed a separate set of experiments in which we interrupted the alignment process at several stages and measured the dynamic moduli using small strains (Appendix). As was the case of perpendicular alignment, there is a monotonic drop in G' and G'' associated with the changes that occur during the first few hundred seconds of large-amplitude shearing at either 100 or 10 rad/s (up to point c in Figure 4a). The dynamic moduli hardly change from point c to point d and then drop again on proceeding to point e. Given the very different orientation distributions indicated by the birefringence at these points for the 10 and 100 rad/s cases, the dynamic moduli at corresponding points in the processes are surprisingly similar.

C. Effect of Shear Frequency on Alignment. The flow alignment experiments carried out at 100, 10, and 1 rad/s clearly suggest that distinct processes dominate at each of the three frequencies, leading to different trajectories of the birefringence and different final aligned states. In this section we focus on two issues: the effect of ω on the development of similar final aligned states through dramatically different evolution pathways, *i.e.*, 10 rad/s $\leq \omega \leq$ 100 rad/s, and the effect of ω on the orientation direction induced by shearing, *i.e.*, 1 rad/s $\leq \omega \leq$ 10 rad/s.

1. Effect of Frequency on the Development of Parallel Alignment. As the shear frequency is decreased from 100 to 10 rad/s, the evolution of the birefringence shows a monotonic progression from having a negative extremum to a positive maximum (Figure 5). A strain amplitude[39] of $\gamma_0 = 0.5$ was used for frequencies ranging from 60 to 20 rad/s. For some of the cases examined (*e.g.*, $\omega = 30$ rad/s, $\gamma_0 = 0.5$), the displacement of the birefringence remains near zero throughout the process. Yet in every case, the effective moduli G'_{eff} and G''_{eff} during the alignment process showed the characteristic large drop initially and a final flattening out. Large-amplitude shearing was continued until both G^*_{eff} and $\Delta n_{13}^{(d)}$ had reached constant values. For all ω from 10 to 100 rad/s, the ultimate value of $\Delta n_{13}^{(d)}$ was approximately zero and the dynamic moduli

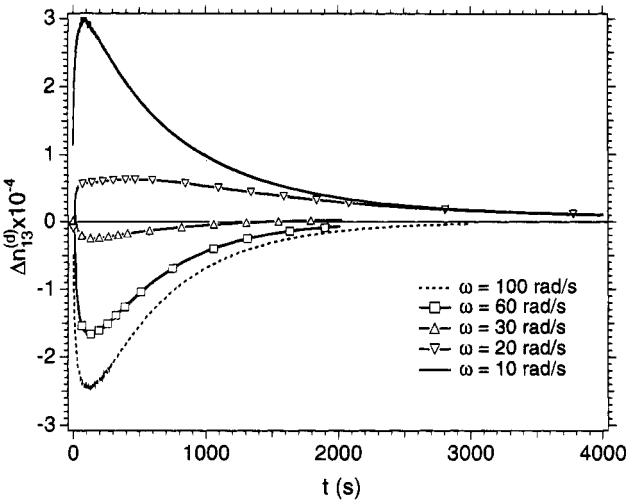

Figure 5. Evolution of the steady offset in 1,3-birefringence during large-amplitude shear alignment at T_0 = 120 °C for frequencies 100−10 rad/s to a parallel aligned state. Strain amplitude $\gamma_0 = 0.8$ was used at 10 rad/s, and $\gamma_0 = 0.5$ for 100−20 rad/s.[39]

after shearing were the same and roughly an order of magnitude lower than that in the initial unaligned condition. Both $\Delta n_{13}^{(d)} \approx 0$ and low $G^*(\omega)$ of the final state suggest that parallel alignment was induced in all cases.

2. Effect of Frequency on the Direction of Alignment. To examine alignment behavior at a frequency lying between the dominant parallel (*i.e.*, $\omega \geq 10$ rad/s) and perpendicular (*i.e.*, $\omega \leq 1$ rad/s) regimes,[40] we performed shear alignment at 4 rad/s. Oscillatory shear at $\gamma_0 = 0.4$ resulted in buildup of a large positive birefringence,[41] typical of perpendicular alignment (Figure 3a). During flow, G^*_{eff} showed a modest initial decrease and then became relatively constant (Figure 6a; *cf.* Figure 3b). The dynamic moduli of the final aligned state (Figure 6b) were identical to those of a perpendicular aligned sample (Figure 3c).

In contrast, shearing at the same frequency and temperature but using $\gamma_0 = 1.1$ induced parallel alignment as indicated by a near zero final $\Delta n_{13}^{(d)}$ (Figure 2a in Gupta *et al.*[41]) and small strain moduli after alignment (Figure 6c) consistent with those of parallel aligned material (Figures 4c). The time trace of $\Delta n_{13}^{(d)}$ was similar to the behavior at 10 rad/s, but reaching a significantly higher maximum value of $\Delta n_{13}^{(d)} \approx 4.2 \times 10^{-4}$ before decaying to zero. The effective dynamic moduli recorded during flow alignment showed significant differences from that observed at $\gamma_0 = 0.4$ (Figure 6a): the decreases of both G'_{eff} and G''_{eff} were larger than the modest decreases observed during alignment at $\gamma_0 = 0.4$. Instead, the behavior was similar to that observed during parallel alignment at 10 rad/s (Figure 4b).

4. Discussion

A. Monitoring the Alignment Process. To achieve a fundamental understanding of the flow alignment process, it is essential to record material properties that sensitively reflect changes occurring during alignment. In most previous studies, no measurement of stress or microstructure was made during shearing. In a few cases the stress has been recorded during the process.[4,10−12,17] In addition, numerous authors have noted the effects of alignment on the small-strain

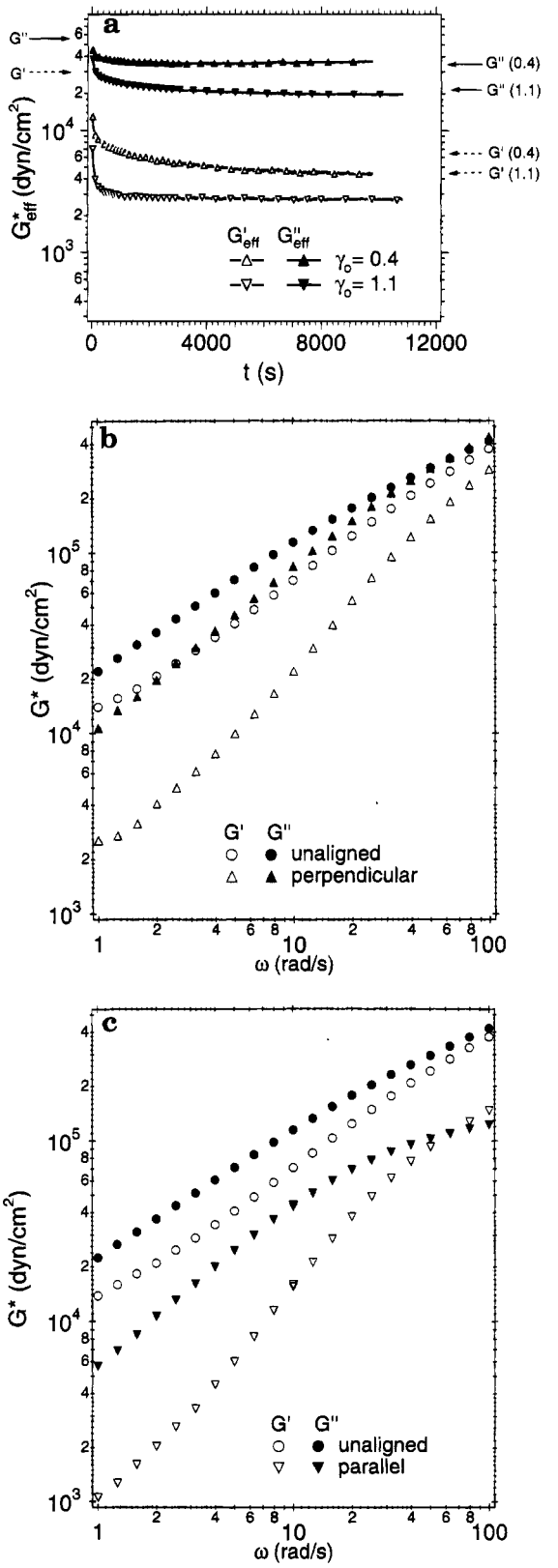

Figure 6. (a) Evolution of effective storage and loss moduli corresponding to the large-amplitude shear alignment experiments at 4 rad/s, $\gamma_0 = 1.1$ and $\gamma_0 = 0.4$ (evolution of birefringence is described elsewhere[41]). Sparsely spaced markers have been used to distinguish between the curves. The arrows at the left and right indicate the small strain dynamic moduli before and after shearing with the strain amplitude indicated (0.4 or 1.1). (b and c) Dynamic moduli obtained using small strain oscillatory shear measurement before and after large-amplitude shear as in part a.

dynamic moduli.[4-6,10-12,17] These raise the question whether either the effective moduli (or viscosity) during the alignment process or the dynamic moduli at intermediate states of alignment can provide a means to monitor microstructural changes in the sample. In our experiments, neither G^*_{eff} nor $G^*(\omega)$ at intermediate stages sensitively reflects microstructural changes. In contrast, the transient birefringence dramatically reveals the evolution of the microstructure during flow alignment.

Dynamic Moduli. In all the cases examined for both alignments, G^*_{eff} goes through an initial drop which is only modestly larger en route to parallel alignment than to perpendicular (Figures 3b, 4b, and 6a). Following this drop, G^*_{eff} shows little change in magnitude compared to the significant changes in the magnitude of $\Delta n^{(d)}_{13}$. Thus, even though the microstructure changes significantly during this time, it does not substantially alter G^*_{eff}.

Low-strain dynamic moduli, $G^*(\omega)$, measured at intermediate states of alignment show only slight sensitivity to the evolution of the microstructure during shear and the changes in $G^*(\omega)$ can be nonmonotonic. Variations in both G' and G'' are gradual for a large part of the alignment process (Appendix), in spite of considerable changes in the microstructure as revealed by the birefringence. Microstructures with very different orientation distributions appear to have essentially the same $G^*(\omega)$. Thus, even if the relationship between microstructure and $G^*(\omega)$ were known, it would be impossible to infer the orientation distribution from $G^*(\omega)$.

Birefringence. In the present system (PS−PI) the form effect dominates the birefringence, so the birefringence is directly related to the second moment of the orientation distribution of the lamellae. To a good approximation, the deviatoric parts of the refractive index tensor ($\Delta\mathbf{n}$) and the order parameter tensor $\mathbf{S}$ are proportional:

$$\Delta\mathbf{n} = -n_0(\mathbf{S} - \mathbf{I})$$

where $S_{ij} = \langle u_i u_j \rangle$, with $\mathbf{u}$ being the normal to the lamellae and $\langle ... \rangle$ denoting an average over the orientation distribution, $\mathbf{I}$ is the identity tensor, and n_0 is a constant of proportionality that depends on the strength of segregation and the resulting periodic variation of the mean refractive index. Empirically, n_0 can be determined from birefringence measurements in samples in which the orientation distribution is known. We estimate the value of n_0 for the present sample at 120 °C by the largest birefringence we have ever observed for a perpendicular aligned sample, $\Delta n_{max} \simeq 10 \times 10^{-4}$. Using TEM we are currently characterizing the orientation distribution in samples that show such high birefringence values. We believe this value of n_0 corresponds to a very highly aligned state since it is more than half the value observed and calculated for strongly segregated PS−PI, which should consequently have a much larger value of n_0 than the present samples. Therefore, we will frequently compare the birefringence of samples to this benchmark value.

Complete characterization of $\mathbf{S} - \mathbf{I}$ requires the value of n_0 and measurement of at least two projections of the refractive index tensor. In the present experiments, we are limited to observing just one projection.[42] Therefore, we can provide bounds on the orientation distribution and make reasonable inferences about the trajectory of orientation. Ongoing TEM and SAXS measurements on samples removed at intermediate states of alignment will provide the basis for more definitive interpretation.

Large 1,3-birefringence values provide relatively unambiguous results. In particular, $n_{11} - n_{33} = n_0$ can only correspond to an order parameter tensor with $S_{33} = 1$ as its only nonzero component. This corresponds to perfect perpendicular alignment. Similarly, $n_{11} - n_{33} = -n_0$ can only mean $\mathbf{S}$ has $S_{11} = 1$ as its only nonzero component, which would correspond to perfect transverse alignment. The interpretation becomes more ambiguous as the birefringence decreases. Observing zero birefringence in the 1,3-plane can correspond to any uniaxial distribution

$$\mathbf{S} = \begin{bmatrix} \epsilon/2 & 0 & 0 \\ 0 & 1-\epsilon & 0 \\ 0 & 0 & \epsilon/2 \end{bmatrix}$$

Here, we have neglected $S_{12} = S_{21}$ since it averages to zero over a cycle of shear (an odd function of strain); in the present flow geometry, S_{13}, S_{31}, S_{23}, and S_{32} are zero by symmetry. The initial, unaligned state with a random grain orientation distribution corresponds to the case $\epsilon = 2/3$; and a perfect parallel alignment corresponds to $\epsilon = 0$. Therefore, in our experiments, when the birefringence is small, we take into account the dynamic modulus, previous SAXS and TEM studies on similar materials, and context within an overall trajectory.[10-12]

B. Route to Alignment. Upon application of large-amplitude shear, distinct changes in the orientation distribution occurring at vastly different time scales are evident in the evolution of birefringence. During both parallel and perpendicular alignments, we observe an initial "fast" and a subsequent relatively "slow" change in the transient birefringence. In each of these processes, the time scale of the changes in birefringence shows distinct dependencies on strain amplitude.[38] The initial fast process is accompanied by a large drop in the effective modulus during shear; during the slow process G^*_{eff} is relatively flat.

The initial condition on each experiment is obtained by annealing at a temperature above the microphase transition temperature (*i.e.*, T_{ODT}) and then cooling to 120 °C in the ordered state. We expect that the resulting sample morphology consists of randomly oriented lamellar grains.[11] The order parameter tensor in this state can be described as $S_{11} = S_{22} = S_{33} \simeq 1/3$, which is consistent with the near zero 1,3-birefringence observe prior to large-amplitude shear.[21] Flow-induced changes in the lamellar orientation distribution (or the order parameter tensor) can be visualized from the transient birefringence, guided by its sign and magnitude.

Perpendicular Alignment. Large-amplitude shearing at 1 rad/s at $T = 120$ °C produces a rapid positive rise in $\Delta n^{(d)}_{13}$ (Figure 3a). This "fast process" can be interpreted as a dominant rapid decrease of S_{11} relative to S_{33}, indicating depletion of the grains biased toward the transverse (axis 1) direction. Furthermore, during this initial fast process the birefringence reaches point c ($\sim(2/3)\,\Delta n_{max}$) on Figure 3a within ~600 s. This large magnitude of $\Delta n^{(d)}_{13}$ strongly suggests a simultaneous rapid increase of S_{33}, *i.e.*, the projection of the orientation distribution along the perpendicular direction (axis 3). Thus, at point c, the order parameter tensor corresponds to grain orientations distributed across parallel and perpendicular directions, with the latter dominating.

Beyond point c, a much slower perfection of the alignment occurs, indicated by a gradual increase in $\Delta n_{13}^{(d)}$ toward n_0. This may correspond to gradual depletion of the projection of the orientation distribution in the parallel direction ($S_{22} \rightarrow \sim 0$) and a final alignment along the perpendicular direction ($S_{33} \rightarrow \sim 1$).

Parallel Alignment. During alignment at frequencies from 100 to 10 rad/s, unambiguous interpretation of the trajectory of alignment from 1,3-birefringence is difficult. However, here the small-strain moduli measurements at intermediate stages (Appendix) and in the final aligned state complement the birefringence measurements and allow visualization of the trajectory of alignment.

At 100 rad/s (Figure 4a), the initial rapid decrease in $\Delta n_{13}^{(d)}$ to approximately $-(1/3)n_0$ suggests a rapid depletion of the projection along the perpendicular direction ($S_{33} \sim 0$) while the projection along the transverse direction remains relatively unchanged from the initial isotropic state ($S_{11} \sim 1/3$). Since both $G'(\omega)$ and $G''(\omega)$ at point a on Figure 4a are considerably smaller than those of the unaligned material (Appendix)—quite unlike the case of perpendicular alignment—we infer that the projection along the parallel direction is enhanced. In contrast, the rapid rise of $\Delta n_{13}^{(d)}$ at 10 rad/s (Figure 4a) to approximately $(1/3)n_0$ indicates that here $S_{11} \rightarrow \sim 0$, while S_{33} remains unchanged and S_{22} increases.

At frequencies from 60 to 20 rad/s, the initial fast change is much less apparent and $\Delta n_{13}^{(d)}$ remains close to zero. In the context of a final parallel alignment, this would indicate that the projections along both perpendicular and transverse directions decrease at comparable rates (Figure 5). In all cases, *i.e.*, 10−100 rad/s, at the end of the initial fast process the order parameter tensor corresponds to an orientation distribution depleted in its projection along either perpendicular (at 100 rad/s) or transverse directions (at 10 rad/s), or both (60−20 rad/s), and increased projection along the parallel direction.

As in the case of perpendicular alignment, during the slower process the direction of alignment is perfected, with the final value of $\Delta n_{13}^{(d)} \approx 0$ indicating an almost complete disappearance of the projection of the orientation distribution in the 1,3-plane.

Effect of Frequency and Strain on Routes to Alignment. Shear frequency appears to play a decisive role in selecting the route to either parallel or perpendicular alignment. In particular, for the initial fast change during shearing at 120 °C:

1. For $\omega \geq 30$ rad/s, S_{33} decreases relative to S_{11}, while S_{22} increases.
2. For 10 rad/s $\leq \omega \leq$ 30 rad/s, S_{11} decreases relative to S_{33}, while S_{22} increases.
3. For $\omega = 1$ rad/s, S_{11} decreases relative to S_{33}, while S_{33} increases.

As shearing frequency is reduced from 10 to 1 rad/s, the character of the "fast" alignment process shifts from enriching the parallel to enriching the perpendicular projection at the expense of the transverse projection of the orientation distribution. Such a shift is also reflected in results during shearing at 4 rad/s. Enrichment of the perpendicular projection during the fast process, for both $\gamma_0 = 0.4$ and 1.1, is indicated by transient birefringence that exceeds $(1/3)n_0$.[41]

During the subsequent slower process at 4 rad/s, strain plays a critical role—selecting the ultimate direction of alignment: for $\gamma_0 = 1.1$, the perpendicular projection disappears during the slow process, while for $\gamma_0 = 0.4$, the parallel projection decreases. At other frequencies, the effect of strain on the slow process is also profound: below a critical strain, the slow process appears not to occur, and the alignment is never perfected.[38]

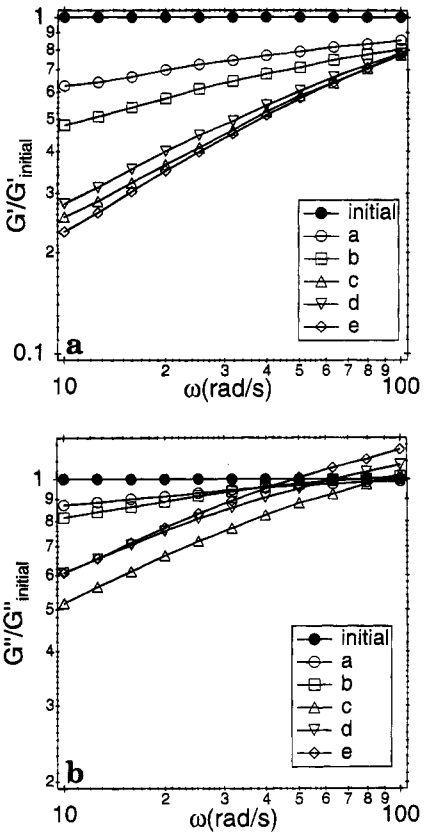

Figure 7. Small-strain measurements of (a) storage and (b) loss moduli at various intermediate points during shear alignment at 1 rad/s. At each frequency, G' and G'' are normalized by the respective modulus before shear alignment.

C. Implications on Alignment Mechanisms. The observation that the rate of disappearance of grains with layer normals along the vorticity direction (*i.e.*, perpendicular direction) can surpass that for the transverse grains is extremely surprising, since almost all previous studies presume that the grains with a dominant normal projection along the transverse direction are the most unfavorable.[5,8,13] It has been argued that, since these layers would be compressed, they are unstable and disappear rapidly either by rotation or melting or some combination of the two. As mentioned previously, almost all of these earlier studies involve characterization of the microstructure at the end of the alignment process and formulation of a mechanism based on those observations. From solely postalignment characterization, the samples shear aligned at the 100 and 10 rad/s exhibit identical final states. It is only from the *in-situ* transient birefringence measurement that we are able to distinguish between the two very different trajectories.

This result has profound implications regarding the concept of selective grain melting suggested to explain the disappearance of the domains biased in "unfavorable" orientations. It has been speculated that the perpendicular orientation is the least susceptible to grain melting.[5] In our experiments during shear alignment at the highest frequencies, *i.e.*, 30−100 rad/s, the grains biased along the perpendicular direction disap-

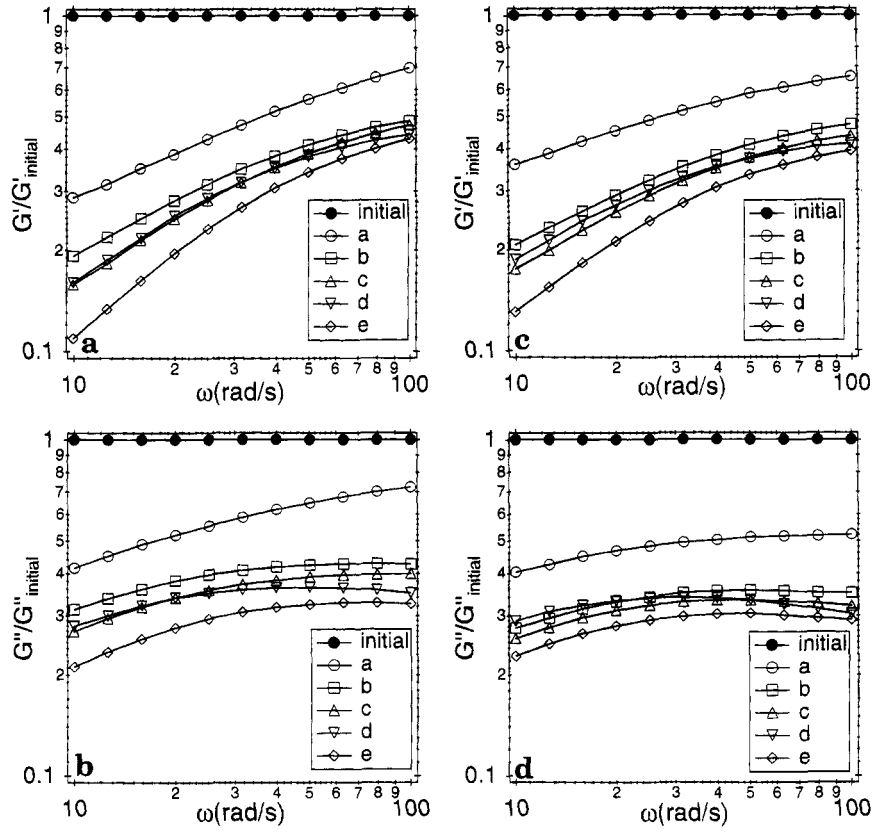

Figure 8. Small-strain measurements of storage and loss moduli at various intermediate points during shear alignment at (a and b) 10 and (c and d) 100 rad/s. At each frequency, G' and G'' are normalized by the respective modulus before shear alignment.

pear more rapidly than all others, particularly relative to those along the transverse direction. Therefore, in this frequency regime, we would expect that grain melting is not the dominant mechanism of flow alignment to a final parallel state. In addition, selective layer melting has been invoked to explain selection of a final perpendicular aligned state. However, results of alignment at 4 rad/s show that oscillatory shear at the larger strain amplitude ($\gamma_0 = 1.1$) induces parallel alignment and at the lower strain amplitude ($\gamma_0 = 0.4$) induces perpendicular alignment. One would expect that at the higher strain amplitude, which corresponds to a higher distortion of equilibrium layer spacing and greater disturbance of fluctuations, selective grain melting would lead to an even better perpendicular alignment, which is not the case. Thus, while grain melting may occur here, it cannot be the only mechanism determining the final state of alignment.

As in earlier studies[3,4] shearing is correlated with a reduction in the modulus, both during shear and after alignment. However, this reduction of the modulus does not appear to underlie the selection between parallel and perpendicular alignment. Contrary to recent suggestion,[43] in this PS–PI, consideration of the small-strain moduli would only yield parallel alignment, which is the lower modulus throughout the frequency range in our experiments. It could be argued that, during large-amplitude shear, the effective dynamic modulus would play a controlling role in determining the final direction of alignment. However, it is seen clearly that the greatest reduction in the effective modulus occurs within the first few hundred seconds of shear, while the microstructure is still far from macroscopic alignment in a particular direction. Furthermore, parallel alignment is consistently associated with a larger decrease in G^*_{eff}—yet it is not the preferred direction of alignment at all shear frequencies. Even at the same shear frequency (4 rad/s), different strain amplitudes lead to different final states of alignment[41] even though a lower effective modulus during shearing is associated with the trajectory to parallel alignment (Figure 6a).

As has been suggested by numerous investigators, defects may play a key role in determining the alignment direction. If these become the dominant stress-bearing structures only at very low frequencies, it could be argued that our shear alignment experiments are restricted to frequencies much higher than those where defect motion may dominate stress relaxation and that alignment is not a direct result of these long-range dynamic modes. However, it still is not clear what defines this time scale for defect mobility and how it is affected by frequency and strain. As our birefringence measurements do not yield information on defect structures, we plan to investigate this aspect using TEM to characterize the morphology and thereby the nature and distribution of defects at intermediate stages of alignment.

5. Summary

The evolution of the microstructure during flow alignment can be monitored using rheooptical techniques. In particular, *in-situ* birefringence measurements reveal changes in the microstructure very sensitively, while the modulus is relatively insensitive. The transient birefringence during shear shows an initial fast change in the orientation distribution, followed by a "slower" refinement that perfects the final aligned state. During the initial fast process, rapid depletion of the projections of the orientation distribution along either the perpendicular or the transverse directions occurs. We find that the relative depletion rates of these two projections depend on the shear frequency. Con-

trary to literature, shear alignment is not always accompanied by a rapid disappearance of lamellae oriented in the transverse direction.

Our results indicate the need for a more rigorous examination of the simple concepts put forth in literature to explain flow-induced alignment. We find that there is a complex interplay among shear frequency and strain in controlling the microstructure and affecting the relaxation dynamics. The previously neglected strain amplitude plays an important role in flow-induced alignment of lamellar block copolymers, affecting not only the alignment kinetics but also the direction of final alignment.

Acknowledgment. This research was carried out with the support of the NSF-PYI (J.A.K.), Chevron, and Raychem. We thank Dr. Steven Paulin for helpful discussions.

Appendix

To observe the relationship between changes in the microstructure and the relaxation behavior, small-strain moduli were measured at different stages during alignment. During the stoppage of large-amplitude shearing the birefringence relaxed slightly (<5%) while each small-strain frequency sweep was performed. However, once large-amplitude shearing was resumed, the birefringence rapidly reached the value just before the interruption of large-amplitude shearing. It then followed a trajectory similar to that observed when shearing was continuous. The magnitude of the recovery in $\Delta n_{13}^{(d)}$ during the pause for small-strain experiments decreased with shearing time, being the largest when shearing was stopped at the end of the fast process (point a in Figures 3a and 4a).

For perpendicular alignment, G' shows a monotonic decrease as alignment progresses (Figure 7a). To facilitate comparison, G' and G'' are shown normalized by the corresponding values before shear alignment. Almost all of the change in the frequency dependence of G' occurs as $\Delta n_{13}^{(d)}$ increases to $\sim 6 \times 10^{-4}$ (point c in Figure 3a). The loss modulus shows a different, nonmonotonic behavior (Figure 7b): it decreases only slightly from the initial unaligned state as $\Delta n_{13}^{(d)}$ increases to $\sim 4.5 \times 10^{-4}$ (point b in Figure 3a). However, with further increase of the retardation to $\Delta n_{13}^{(d)} \simeq 6 \times 10^{-4}$ (point c), there is a large drop in G'' to nearly 50% of the initial value at low frequencies. Beyond this, as the birefringence increases, G'' *increases* by about 10–15% equally at all frequencies.

During alignment at 10 and 100 rad/s, almost all the changes in the frequency dependence for both G' and G'' occur in the first 400 s of shearing (Figure 8a–d): in both cases, a large drop in the moduli occurs as $\Delta n_{13}^{(d)}$ passes its extremum and drops to an absolute value of $\sim 2.2 \times 10^{-4}$ (point b). Beyond this point, both G' and G'' show a gradual monotonic decrease.

References and Notes

(1) Bates, F. S.; Fredrickson, G. H. *Annu. Rev. Phys. Chem.* **1990**, *41*, 525. Bates, F. S. *Science* **1991**, *251*, 898. Bruinsma, R.; Rabin, Y. *Phys. Rev. A* **1992**, *45*, 994. Safinya, C. R.; Sirota, E. B.; Bruinsma, R. F.; Jeppesen, C.; Plano, R. J.; Wenzel, L. J. *Science* **1993**, *261*, 588. Idziak, S. H. J.; Safinya, C. R.; Hill, R. S.; Kraiser, K. E.; Ruths, M.; Warriner, H. E.; Steinberg, S.; Liang, K. S.; Israelachvili, J. N. *Science* **1994**, *264*, 1915.

(2) Keller, A.; Pedemonte, E.; Willmouth, F. M. *Colloid Polym. Sci.* **1970**, *238*, 25. Folkes, M. J.; Keller, A.; Scalisi, F. P. *Colloid Polym. Sci.* **1973**, *251*, 1. Hadziioannou, G.; Mathis, A.; Skoulious, A. *Colloid Polym. Sci.* **1979**, *257*, 136.

(3) Hadziioannou, G.; Mathis, A.; Skoulious, A. *Macromolecules* **1982**, *15*, 258.

(4) Morrison, F. A.; Winter, H. H. *Macromolecules* **1989**, *22*, 3533. Morrison, F. A.; Winter, H. H.; Gronski, W.; Barnes, J. D. *Macromolecules* **1990**, *23*, 4200.

(5) Koppi, K.; Tirrel, M.; Bates, F. S.; Almdal, K.; Colby, R. H. *J. Phys. II* **1992**, *2*, 1941.

(6) Koppi, K.; Tirrel, M.; Bates, F. S. *Phys. Rev. Lett.* **1993**, *70*, 1449.

(7) Amundson, K.; Helfand, E.; Davis, D. D.; Quan, X.; Patel, S. S.; Smith, S. D. *Macromolecules* **1991**, *24*, 6546. Amundson, K.; Helfand, E.; Quan, X.; Smith, S. D. *Macromolecules* **1993**, *26*, 2698.

(8) Amundson, K.; Helfand, E. *Macromolecules* **1993**, *26*, 1324.

(9) Amundson, K.; Helfand, E.; Quan, X.; Hudson, S. D.; Smith, S. D. *Macromolecules* **1994**, *27*, 6559.

(10) Winey, K. I.; Patel, S. S.; Larson, R. G.; Watanabe, H. *Macromolecules* **1993**, *26*, 2542.

(11) Winey, K. I.; Patel, S. S.; Larson, R. G.; Watanabe, H. *Macromolecules* **1993**, *26*, 4373.

(12) Larson, R. G.; Winey, K. I.; Patel, S. S.; Watanabe, H. *Rheol. Acta* **1993**, *32*, 245.

(13) Kornfield, J. A.; Kannan, R. M.; Smith, S. D. *Abstr. Pap—Am. Chem. Soc.* **1994**, *71*, 250.

(14) Zhang, Y.; Wiesner, U.; Spiess, H. W. *Macromolecules* **1995**, *28*, 778.

(15) Bates, F. S.; Rosedale, J. H.; Bair, H. E.; Russell, T. P. *Macromolecules* **1989**, *21*, 2557.

(16) Rosedale, J. H.; Bates, F. S. *Macromolecules* **1990**, *23*, 2329.

(17) Kannan, R. M.; Kornfield, J. A. *Macromolecules* **1994**, *27*, 1177.

(18) Balsara, N.; Hammouda, B.; Kesani, P. K.; Jonnalagadda, S. V.; Straty, G. C. *Macromolecules* **1994**, *27*, 2566. Balsara, N. P.; Hammouda, B. *Phys. Rev. Lett.* **1994**, *72*, 360.

(19) Okamoto, S.; Saijo, K.; Hashimoto, T. *Macromolecules* **1994**, *27*, 5547.

(20) We performed a temperature sweep at a rate of 1 °C/min and in steps of 1 °C. At each temperature the dynamic moduli were measured using oscillatory shear at 10 rad/s and 2% strain. At T_{ODT}, both moduli (G', G'') exhibited a steep decrease, which was more pronounced for G'. Similar determination revealed a typical hysteresis behavior upon cooling with the transition temperature a few degrees lower than that during heating. The order–disorder transition temperature is also manifested in optical measurements as a steep decrease in the "apparent birefringence".[21] For yet unknown reasons, we observed T_{ODT} of 171 and 164 °C for two different batches for the same polymer sample. All the experiments reported in this paper were performed with the latter.

(21) In the microphase-separated state for block copolymers a small apparent birefringence results from depolarization of the polarized light upon transmission through a collection of randomly oriented lamellar grains.

(22) Kannan, R. M.; Kornfield, J. A. *Rheol. Acta* **1992**, *31*, 535.

(23) Kannan, R. M.; Kornfield, J. A.; Schwenk, N.; Boeffel, C. *Macromolecules* **1993**, *26*, 2050.

(24) Surface ordering effects have been observed in the literature.[18] We are unable to comment on these from our birefringence measurements. On the basis of the random morphology studied by Winey *et al.*,[11] we interpret the initial state as unaligned.

(25) The ratio of the 3ω component to the 1ω component in the stress response, during most of the shear alignment process, was within 1%. At 10 and 1 rad/s, it was approximately 10% at the start of shear but decreased rapidly to a value less than 1% within the first few cycles. In contrast, at 100 rad/s, this ratio increased from an initial value of about 3% to 5% and then decreased rapidly to a value less than 1%. The 5ω component was an order of magnitude smaller throughout the alignment.

(26) Lodge, T. P.; Fredrickson, G. H. *Macromolecules* **1992**, *25*, 5643.

(27) Allan, P.; Arridge, R. G. C.; Ehtaiatkar, F.; Folkes, M. J. *J. Phys. D: Appl. Phys.* **1991**, *24*, 1381.

(28) Almdal, K.; Bates, F. S.; Mortensen, K. *J. Chem. Phys.* **1992**, *96*, 9122.

(29) Bates, F. S.; Rosedale, J. H.; Fredrickson, G. H. *J. Chem. Phys.* **1992**, *92*, 6255.

(30) A near zero birefringence can be ambiguous, since it can correspond to any state that has a symmetric distribution about the velocity gradient direction [*e.g.*, parallel alignment, an isotropic distribution of the lamellar grains (either overall or in the 1,3-plane) or a collection of onion-like structures

(observed in lamellar lyotropics[31])]. Therefore, we interpret $\Delta n_{13}^{(d)}$ in the context of the overall alignment trajectory and in combination with the changes in the mechanical properties (G', G'') of the sample. We also draw on previous structural studies using TEM/SAXS for a very similar polymer system,[10] which clearly establish the existence of aligned lamellar morphology after large-amplitude oscillatory shear and correlate the aligned state with changes in G' and G''.

(31) Diat, O.; Roux, D.; Nallet, F. *J. Phys. II (Fr.)* **1993**, *3*, 1427.

(32) Testing at $T \leq 110$ °C (*i.e.*, $5.5 \leq a_T\omega$ [rad/s] $\leq 66 \times 10^3$) was performed with $\gamma_0 \leq 0.003$. For $T \leq 130$ °C (*i.e.*, $1 \leq a_T\omega$ [rad/s] ≤ 24), strains with $\gamma_0 \leq 0.02$ were used. Higher temperatures required larger strains; by $T \simeq 160$ °C, strains as large as 12% were used at the lowest ω. At $T \geq 164$ °C the material is disordered and linear behavior is observed for all strain amplitudes used.

(33) It was not possible to superimpose the results of the frequency sweep [100−10 rad/s ($\gamma_0 = 0.03$) and 10−1 rad/s ($\gamma_0 = 0.12$)] at 160 °C (Figure 2a). This could be due to the increasing strength of composition fluctuations as T_{ODT} is approached.[16,28,29] The discontinuity in G' at the overlap frequency of 10 rad/s is due to the nonlinear effect of strain amplitude.

(34) Kawasaki, K.; Onuki, A. *Phys. Rev. A* **1990**, *42*, 3664.

(35) Rubinstein, M.; Obukhov, S. P. *Macromolecules* **1993**, *26*, 1740.

(36) Parallel alignment in PS−PI has also been recently reported at frequencies lower than those corresponding to perpendicular alignment.[14] However, in our experiments, shearing at a lowest reduced frequency of $a_T\omega \sim 0.0034$ rad/s ($\omega \approx 0.1$ rad/s at 150 °C) and $\gamma_0 \simeq 1.5$ still produced perpendicular alignment.[38]

(37) Bloss, F. D. *An Introduction to the Methods of Optical Crystallography*; Holt, Rhinehart and Winston, Inc.: New York, 1961.

(38) Gupta, V. K. Krishnamoorti, R.; Kornfield, J. A.; Smith, S. D. In preparation.

(39) At higher frequencies the commanded strain γ_{com} was different than the applied strain γ_a, which varied over the course of prolonged shear. In the figures and text the strain amplitude indicated is the commanded strain. During shear alignment at 100 rad/s, $\gamma_{com} = 0.5$, and the initial strain amplitude was 0.38 and the final 0.44. Corresponding values for other shear frequencies are 60 ($\gamma_{com} = 0.5$, $\gamma_a \simeq 0.44-0.46$), 30 ($\gamma_{com} = 0.5$, $\gamma_a \simeq 0.48$), and 20 rad/s ($\gamma_{com} = 0.5$, $\gamma_a \simeq 0.47-0.485$). Below 20 rad/s, the agreement between the commanded and the applied strain is within 1%.

(40) Shear alignment over a wide range of strains at 10 and 100 rad/s led to dominant parallel alignment and at 1 rad/s to dominate perpendicular alignment. The results of these experiments will be presented elsewhere.[38]

(41) Gupta, V. K.; Krishnamoorti, R.; Kornfield, J. A.; Smith, S. D. Submitted for publication.

(42) For reasonable flow geometries, the 1,2-projection results in a retardation over too many orders due to large path length (~15 mm in our experiments).

(43) Patel, S. S.; Larson, R. G.; Winey, K. I.; Watanabe, H. Submitted to *Macromolecules*.

MA950058B